Seedbed consolidation and surface sealing for soils of different texture and soil organic carbon contents

Nargish Parvin *, Maria Sandin, Mats Larsbo

Swedish University of Agricultural Sciences (SLU), Department of Soil and Environment, P.O. Box 7014 75007, Uppsala, Sweden

ABSTRACT

The soil structure near the surface of agricultural soils changes with season mainly by land management together with climatic and biological factors. Quantitative analysis of post-tillage changes in soil structure and related hydraulic properties are necessary for evaluating and improving models of soil hydrological and transport processes. The objectives of this study were to quantify changes in soil seedbed structure induced by rainfall and drainage and to estimate the eff ;ects of soil texture and SOC on these changes. We collected samples from the harrowed layer of twenty-six fine to coarse textured Swedish mineral soils. Air-dried soil was placed in cylinders (5 cm high, diameter 5 cm) and exposed to simulated rainfall (5 mm h^{-1} for 4 h) and drainage (-50 cm pressure potential) cycles in the laboratory. We used X-ray tomography to quantify changes in pore networks in a thin surface layer and in the whole cylinder. Infiltration rates at -5 cm pressure potential were measured using a mini disc tension infiltrometer on replicate air-dried samples and on the samples included in the consolidation experiments at the final state. Total imaged specific pore volumes generally decreased from initial to final state and pore size distributions were shifted towards larger proportions of below image resolution pores (< 80 μm). There was a strong positive correlation between clay content and changes (i.e. final state-initial state) in the specific volume of pores <80 μm. Soils with high clay content and soil organic carbon (SOC) content often have strong aggregates that resist changes. Nevertheless, both clay and SOC contents were negatively correlated with the changes in specific imaged pore volume. These results highlight the importance of swelling, which is largely controlled by clay content, for seedbed consolidation. In line with previous studies, when excluding coarse textured soil, the changes in surface porosity were negatively correlated with silt content. Changes in infiltration capacity were not significantly correlated with any basic soil properties. Our results suggest that shrinking-swelling should be a central part in any model for seedbed consolidation.

1. Introduction

The soil structure (i.e. the spatial arrangement of solids and pores) at and near the soil surface plays an important role for the distribution of rainfall between surface runoff and infiltration. This, in turn, has a strong influence on water retention, water flows and solute transport in the soil. Soil structure is not constant but changes continuously due to both abiotic and biotic processes (Lin, 2011). For example, soil tillage may within a few seconds completely change the structure of the top 5−6 cm during seedbed preparation. The newly created seedbed returns to its pre-tillage condition in a process referred to as soil consolidation. Soil consolidation is the sum of a number of processes including micro-cracking, swelling and shrinking, aggregate coalescence and slaking that may occur one-at-a-time or simultaneously (Ghezzehei and

Or, 2000; Or and Ghezzehei, 2002; Bresson and Moran, 2004). These processes are induced by wetting-drying and freezing-thawing cycles and by biological activity (Messing and Jarvis, 1993; Franzluebbers et al., 1995; Ahuja et al., 2006; Dörner et al., 2012). Many studies have investigated the effects of consolidation and surface sealing by measuring temporal changes in topsoil hydraulic properties during one or a few growing seasons (Gupta et al., 2006; Alletto and Coquet, 2009; Schwen et al., 2011). Generally, consolidation and surface sealing reduces water infiltration capacity and water retention in the root zone, which influences ground water recharge and increases the risk of surface runoff and soil erosion (Franzluebbers, 2002; Assouline, 2004; Chen et al., 2013; Hiel et al., 2016).

Surface sealing has also been studied extensively using direct methods such as analysis of resin impregnated soil thin sections and X-

---

* Corresponding author.
  E-mail address: Nargish.Parvin@slu.se (N. Parvin).

ray tomography (e.g. Giménez et al., 1992; Valentin and Bresson, 1992; Hyvaluoma et al., 2012; Armenise et al., 2018). Compared to the former methods X-ray tomography has the advantage that a larger soil volume can be analysed and that the 3-D representation allows for quantification of pore network connectivity. Surface sealing occurs when a bare soil surface is directly exposed to rainfall. The impact of raindrops facilitates the breakdown of soil aggregates, dispersion and reorganization of particles leading to the formation of a structural seal, which may have significant effects on hydrological and ecological processes (Franzluebbers, 2002; Assouline, 2004; Assouline and Mualem, 2006). The development of surface seals depends on a wide range of factors such as inherent soil properties (e.g. texture, structure, soil organic carbon (SOC) content), management history, and rainfall characteristics (Assouline, 2004). The most important rainfall characteristic for surface sealing is the kinetic energy of raindrops (Betzalel et al., 1995). However, the effects of drops of similar energy will be very different for soils of contrasting properties. For example, Salles et al. (2000) showed that the rainfall energies needed for particle detachment are generally larger for silt loam soils, which have stronger cohesion between particles compared to sandy soils. Soils with high SOC content tend to have stronger and more stable aggregates (Gronsten and Borresen, 2009) and soils with low SOC content are considered to be most vulnerable to aggregate breakdown and surface sealing (Ramos et al., 2003).

A large number of modelling approaches has been proposed for soil surface sealing (reviewed by Assouline, 2004). However, only a few attempts have been made to model the structural changes occurring during soil consolidation (Ghezzehei and Or, 2000; Or et al., 2000; Maharjan et al., 2018). Direct quantifications of seedbed consolidation are still rare. One example is Sandin et al. (2017) who quantified post-tillage changes in soil pore network in the harrowed layer during one growing season under field conditions using X-ray tomography. Despite the large confounding effects of spatial variability, they found that rainfall events caused significant decreases in imaged porosity within the first month following harrowing. In a follow up laboratory study, Sandin et al. (2018) studied temporal variations in pore network characteristics in seedbeds exposed to artificial rainfall for nine soils with contrasting texture and SOC content. Their results suggested that the magnitude of changes in pore networks could be predicted from basic soil properties. However, to establish such links a larger number of soils would be required. Previous studies have indicated that model predictions of soil water dynamics, solute transport, nutrient cycling and plant growth could be improved by accounting for the temporal variability in the hydraulic properties of tilled soil layers (Schwen et al., 2011; Alletto et al., 2015). Direct measurements of post-tillage soil consolidation and sealing would enable evaluation and parameterization of existing models and possibilities for further development.

The aims of the present study were (i) to quantify changes in soil seedbed structure induced by simulated rainfall and drainage in the laboratory (ii) to estimate the eff ;ects of soil texture and SOC on these changes. To achieve these aims, we measured the structural changes occurring in samples collected directly after harrowing from the seedbeds of 26 mainly fine and medium textured Swedish soils. We used X-ray tomography to directly quantify changes in pore network characteristics in the seedbeds and in a thin surface layer. To relate changes in pore networks to hydraulic properties we also measured unsaturated hydraulic conductivities (at -5 cm pressure potential) on the initial and final states of the seedbeds.

2. Materials and methods

2.1. Soils

Samples were taken in the spring of 2018 from the harrowed layer (0−5 cm depth) of 26 agricultural fields at ten diff ;erent sites in central and northern Sweden (Table S1). All fields were conventionally farmed and had been ploughed to an approximate depth of 25 cm with

mouldboard plough in the previous autumn. However, the conditions prior to seedbed preparation and the equipment used for seedbed preparation were not recorded. All samples were collected within 3 days after harrowing before any rainfall event had influenced the soil structure of the harrowed layer. As the soil in a newly harrowed layer is in a loose and fragmented state it was not considered meaningful to take intact soil cylinders. The samples were, therefore, taken with a trowel. Samples were stored in sealed plastic containers at 3 °C until the start of the experiments, which were carried out in June, July and August 2018. Soils were chosen to cover a wide range of fine and medium textured mineral soils. Clay, silt, sand and SOC content of the samples ranged from 4.2 to 59.4%, 8.9–74.7 %, 4.1–84.3 %, and 10-39.6 g kg^{-1}, respectively (Fig. 1 and Table S1). Particle size distributions were determined by the pipette method and SOC contents were analysed by dry combustion (ISO 10694) on a TruMac CN (LECO Corp.).

2.2. Preparation of soil samples

To create as similar initial conditions as possible we air-dried the samples for five days at 36.5 °C. To reproduce field-like seedbeds each soil sample was first homogeneously spread on a tray and divided into eight parts. Equal amounts of soil were then collected from all eight parts with a spoon and filled into aluminum cylinders (6-cm high, 5.2-cm diameter). The cylinders were shaken very gently to allow the soil to settle. The height of the soil after settling was 5.0−5.2 cm in all cylinders. The cylinders were weighed and sealed at the bottom with polyamide cloth (mesh size 50 μm) to prevent soil loss during the following experiments. Two samples were prepared for each soil. The first set of samples was used for infiltration measurements on air-dried soil (i.e. initial conditions) and the second set was used for the consolidation and surface sealing experiments and for infiltration measurements on consolidated samples (i.e. final conditions).

2.3. Consolidation and surface sealing experiments

The cylinders containing air-dried soil were first imaged using X-ray tomography (see sections 2.5-2.7). The rest of the experiment consisted of two cycles of simulated rainfall using artificial rainwater with an ionic strength of 0.055 mM and pH 5 (Löv et al., 2017) and drainage. Each experimental stage was followed by X-ray imaging. The cylinders were placed in a rainfall chamber where rainfall rates were controlled through individual nozzles placed 90 cm above the soil surface of each cylinder. Rainfall simulations were carried out for 4 h at a constant rate of 5 mm h^{-1}. Raindrops were produced by collecting the fine mist created by the nozzles on 24 copper wires placed below each nozzle. According to Sandin et al. (2018) who used a similar experimental setup,
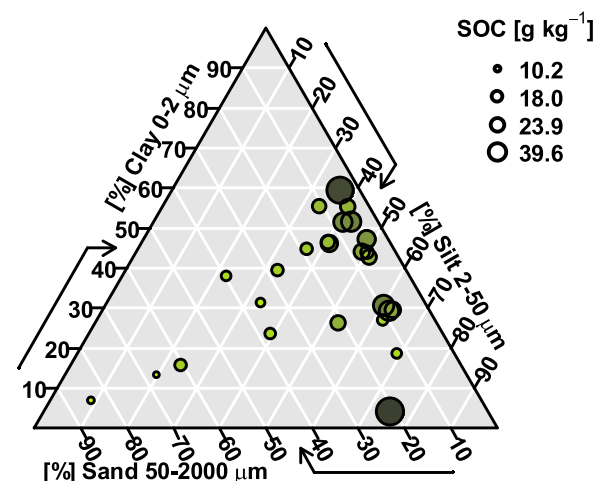

Fig. 1. Soil texture and soil organic carbon (SOC) content of the 26 soils.

the raindrops that formed had a median diameter of approximately 1 mm (estimated from photographs taken during the rainfall simulation) with an estimated kinetic energy of 4.5 J m^{-2} mm^{-1} (calculated based on van Dijk et al., 2002). Each soil sample was placed on a 10-cm high sand column in order to avoid saturated conditions at the bottom of the sample. The sand columns were placed on funnels and were allowed to drain freely at the bottom. After the simulated rainfall, samples remained on the sand column over night to drain any excess water from the soil. The samples were covered to avoid evaporation during this period. On the next day, samples were weighed and imaged. The pressure potential of the samples were then equilibrated on sand beds for at least 5 days at −50 cm pressure potential and then weighed and imaged again. The simulated rainfall followed by drainage and imaging was then repeated resulting in five images for each sample denoted Initial, Rain 1, Drain 1, Rain 2 and Drain 2. The experimental setup is illustrated in Fig. 2.

2.4. Infiltration measurements

Infiltration rates at -5 cm pressure potential were measured using a Decagon mini disc tension infiltrometer on replicate air-dried samples and on the samples included in the consolidation experiments after Drain 2. A thin layer of fine silica sand was applied on the soil to ensure good contact between the soil and the infiltrometer. A stand with a clamp was used to hold the infiltrometer in place and to avoid vertical pressure on the soil sample. After the infiltration measurements the samples from the consolidation and surface sealing experiments were dried in an oven at 105 °C and weighed.

2.5. X-ray tomography imaging

We used the GE Phoenix v|tome|x m X-ray tomograph at the Department of Soil and Environment at SLU. It has a 240 kV X-ray tube, a tungsten target (beryllium window) and a GE 16″ flat panel detector. We collected 2024 radiographs per cylinder. The X ray scans were carried out at a voltage of 120 kV and a current of 400 µA. The exposure time for each radiograph was 250 ms. The pixel edge length was 40 µm. This means that pores larger than approximately 80 µm can be identified in the images. The resulting radiographs were converted to 3-D images using the GE image reconstruction software datos|x and exported as TIFF-stacks (tagged image file format) with 16-bit grey scale resolution.

2.6. Image processing and analysis

Image processing and analyses were carried out using open access software. We used the FIJI distribution (Schindelin et al., 2012) of ImageJ (Abramoff ; et al., 2004) and the ImageJ plugins BoneJ (Doube et al., 2010) and SoilJ (Koestel, 2018). First a 3-D median filter with a 1-pixel radius and an unsharp mask with standard deviation of 1 and a filter weight of 0.6 was used to reduce noise in the grey scale images. We then corrected for radial and vertical differences in illumination in the images using the grey value calibration implemented in SoilJ. A cylindrical region of interest (ROI), which included all voxels enclosed by the inner cylinder wall was then selected. The grey scale images were segmented using the Otsu method (Otsu, 1979) applied to joint histograms for all ROIs as implemented in SoilJ. In order to define the total sample volume, filling of small surface-vented macropores (approximately < 1 mm radius) was done by 13 consecutive 3-D dilations followed by 14 3-D erosions. The resulting image was combined with the original binary image using the logical AND operator. Finally pores below the location of the soil surface were filled to achieve a binary mask containing the sample volume. Grey scale and binary images of the soil matrix, imaged pore network and sample volume of one of the soils (Kungsängen, Table S1) at the initial and final state of the experiments (i.e. Drain 2) are shown in Fig. 3.

A number of measures of the imaged pore networks were calculated from the binary images. To estimate the size of pores we calculated the average pore thickness (TP) using BoneJ (Doube et al., 2010). The thickness of a voxel is the diameter of the largest sphere that fits inside the pore and contains the voxel. In systems where soil volumes are changing, as in our case, it is more convenient to work with specific pore volumes rather than porosities (which by definition depends on the total soil volume). Here, we define the total specific volume of pores as the total volume of pores per mass (g) of dry soil. The specific imaged pore volume (SPV$_{Im,tot}$), the specific volume of pores < 80 µm (SPV$_{<80}$; see section 2.7), 80–320 µm (SPV$_{Small}$), 320–640 µm (SPV$_{Medium}$), and > 640 µm (SPV$_{Large}$) and the specific connected imaged pore volume (see below) were all defined in the same way. The boundaries between imaged pore classes were chosen to achieve, on average, approximately equal pore volumes in all three classes. Similarly, the specific sample volume is given by the total volume of the soil divided by the total mass (i.e. the inverse of dry bulk density). Specific volumes of pores in the surface layer could not be calculated since the mass of soil in that layer
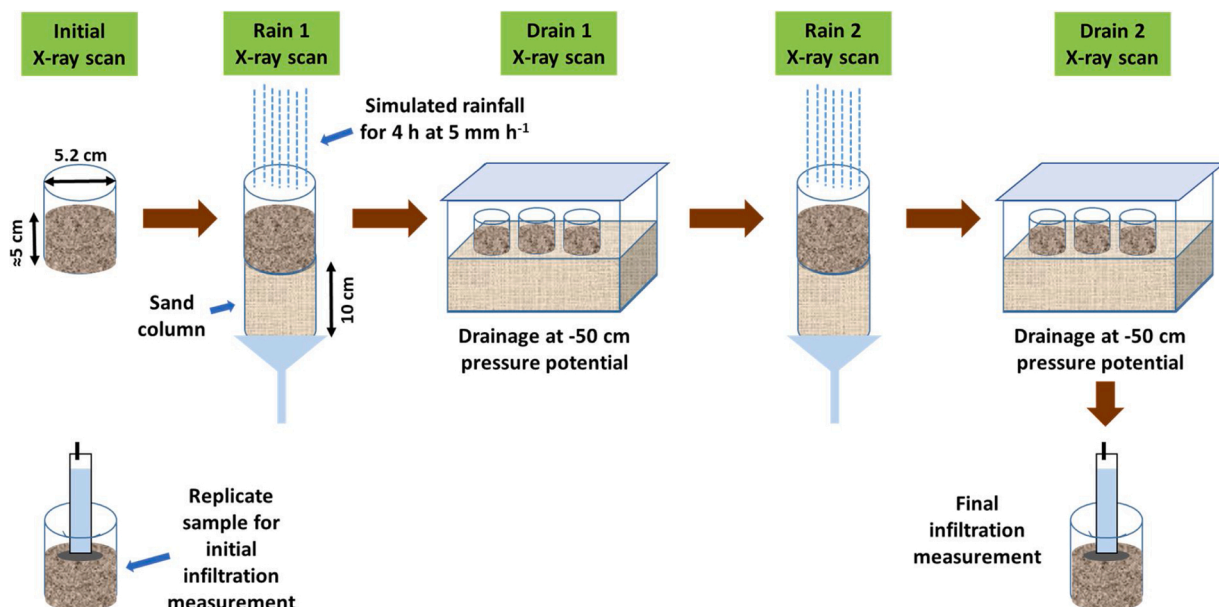

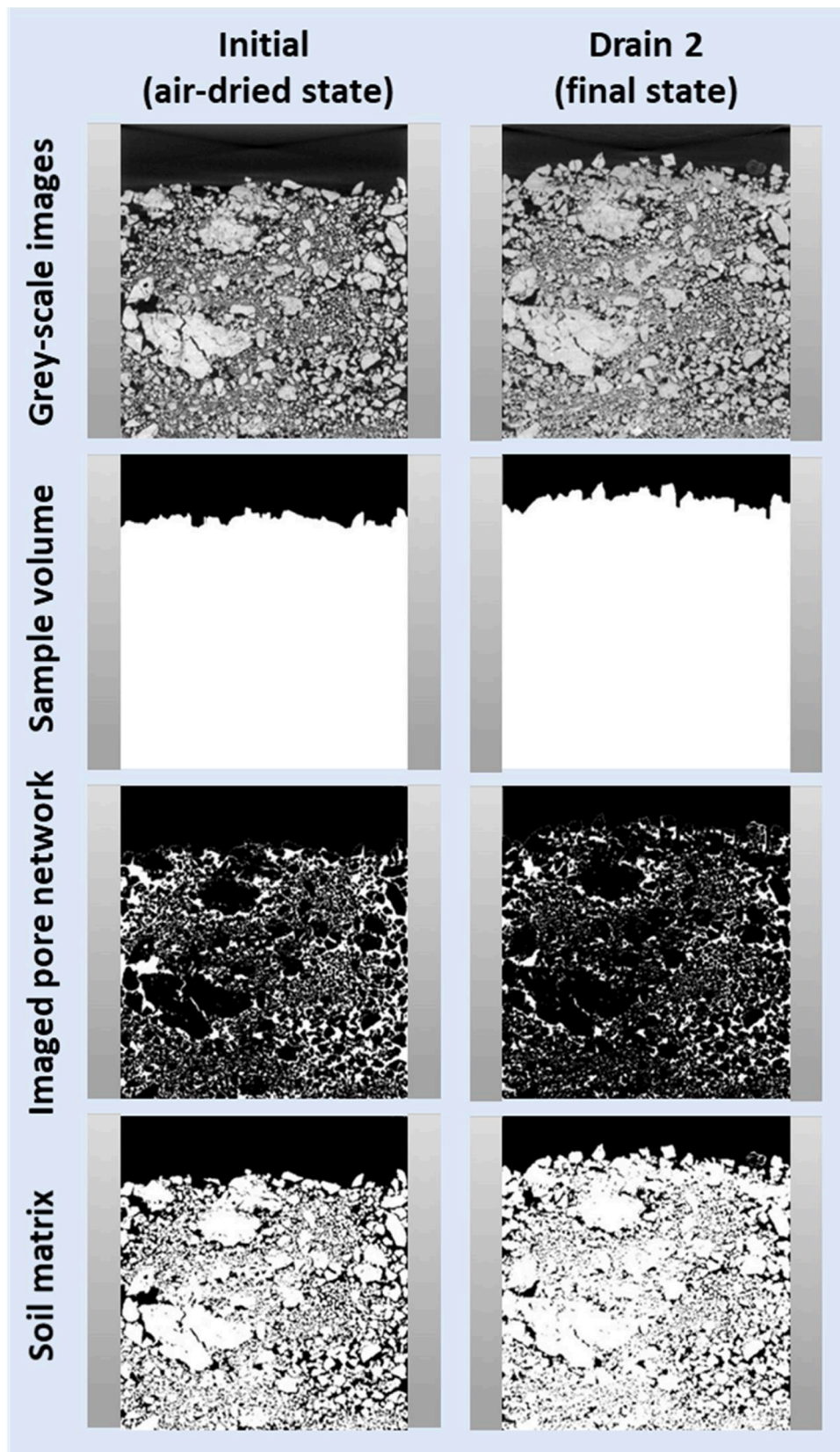**Fig. 2.** Schematic illustration of the experimental setup.

Fig. 3. An example (Kungsängen) of vertical 2-D slices from grey-scale X-ray images and binary images at the experimental stages Initial and Drain 2.

was not known. We, therefore, report imaged near surface porosities (0−1 mm and 1−2 mm depth) calculated using a voxel-counting routine written in R (R Core Team, 2019).

The connectivity of macropores strongly influences hydraulic conductivity and the soil's susceptibility to preferential flow and transport (Hunt, 2013; Jarvis et al., 2017). We calculated four pore network connectivity measures using SoilJ (Koestel, 2018): the specific connected pore volume ($SPV_{Im,conn}$), the percolating fraction (PF), which was given by $SPV_{Im,conn}$ divided by $SPV_{Im,tot}$, the connection probability (Γ), which is the probability that any two arbitrarily chosen pore voxels are connected (Renard and Allard, 2013) and the critical pore diameter (d_{crit}), which is the bottleneck in the pore network that is connected from top to bottom.

2.7. Estimation of below image resolution specific pore volumes

Dry bulk densities of the samples were calculated from the soil volumes (estimated from images) and the sample weights. Then total specific pore volumes (SPV_{tot}) were calculated assuming particle densities of 2.65 and 1.2 g cm^{-3} for mineral and organic matter (Ruhlmann et al., 2006), respectively, and a conversion factor of 1.72 to calculate organic matter content from SOC content. By subtracting the imaged porosity from total porosity a fourth pore size class was obtained which comprised pores smaller than the image resolution of 80 µm ($SPV_{<80}$).

2.8. Statistics

All the statistical analysis were done using either the Pearson or the Spearmen correlation functions in Matlab R2017b (Mathworks Inc.). We created correlation matrices which show the correlations between basic soil properties and pore network characteristics at initial state, final state and for absolute changes in pore network characteristics (i.e. $\Delta p = p_{final} - p_{initial}$, where p is any measure of the pore network). To give the reader a clearer picture of the ranges of measured data we also show graphs of the most important correlations. Correlation analysis were carried out on rank-transformed data (i.e. Spearman correlation coefficients were calculated) for the connectivity measures and for infiltration rates since the original data was not approximately normally distributed. The largest value was assigned rank 1. Regression lines and accompanying R^2-values are given in graphs when the correlations were statistically significant.

3. Results and discussion

3.1. Overall trends

The variation in specific sample volume between samples were large compared to the differences in average specific sample volumes between experimental stages (Fig. 4a). The specific volume of individual samples generally increased (24 of 26 samples) from the initial air-dry state (Initial) to the state following the first simulated rainfall (Rain 1) which shows that swelling was the dominant process during this stage. Between Rain 1 and the final state (Drain 2) changes were smaller with an average decrease in specific sample volume (18 of 26 samples decreased in volume). This shows that other processes than reversible swelling and shrinking, such as slaking, micro-cracking and coalescence, occurred with repeated wetting-drying cycles. These results are very different from the results presented in Sandin et al. (2018) who, in many respects, used a similar experimental setup. One important difference was that, in their study, they first wetted the field moist samples by placing the cylinders in a tray with 1 cm of water for five days. The following drainage to −50 cm pressure potential resulted in a decrease in the sample volumes for 7 of the 9 soils included in their study. In the study by Sandin et al. (2018) the largest changes in pore networks generally took place close to the bottom of the samples whereas soil structural changes, evaluated by visual inspection, were rather homogeneous with depth in our study (not shown). These differences in consolidation between the two studies highlight the importance of the wetting process, where rapid wetting and saturation at the bottom of the sample followed by drainage often led to a decrease in volume while slower wetting from the top followed by drainage mainly resulted in swelling and an increase in sample volume. Effects of wetting rate on the extent of structural changes has also previously been demonstrated for silty soils as well as for soils with larger clay contents (Bresson and Moran, 2004; Mamedov and Levy, 2013).

Fig. 4b shows that the initial increase in specific sample volume was caused by an increase in the specific volume of pores < 80 µm ($SPV_{<80}$) by, on average, 35 %. This increase was larger than the simultaneous decrease by, on average, 25 % for imaged pores ($SPV_{Im,tot}$). This means that pore size distributions were generally shifted towards smaller pore classes. The decrease in specific sample volume from Rain 1 to Drain 2 was due to decreases in specific volumes for both $SPV_{<80}$ and $SPV_{Im,tot}$.

3.2. Correlations between basic soil properties and initial pore network characteristics

Although the focus of this study is on understanding changes in pore networks during surface sealing and consolidation we start by presenting how initial conditions were influenced by soil properties. Changes occurring during seedbed consolidation are known to be dependent on initial conditions (Sandin et al., 2018). A complete correlation matrix for texture, SOC content, initial pore network characteristics and infiltration rates is given in Fig. S1. In the following we highlight the most important correlations. It should be noted that the properties of a seedbed directly after preparation and, hence, also the characteristics of the pore networks, are not solely determined by soil properties but are also influenced by other factors unknown to us, including, for example, the tillage implements used and the soil moisture at seedbed preparation.
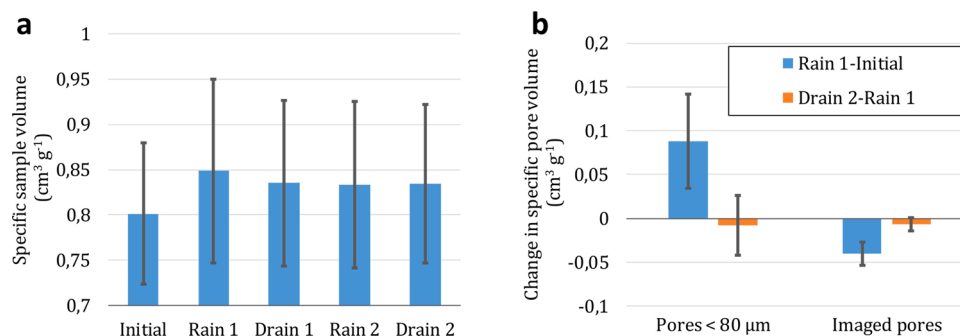

Fig. 4. a) Average specific sample volumes at the five experimental stages and b) changes in specific pore volumes between Rain 1 and the initial state and between Drain 2 and Rain 1 for imaged pores and pores < 80 µm. Error bars indicate two standard deviations.

3.2.1. Specific pore volumes

Total initial specific pore volume (SPV_{tot}) was positively correlated with SOC (Fig. S1). We could not find any studies reporting correlations between basic soil properties and SPV_{tot} for newly prepared seedbeds in the scientific literature, but this result is in line with the effects of SOC on dry bulk densities reported for Swedish agricultural topsoils (e.g. Kätterer et al., 2006) and internationally (Boivin et al., 2009; Emerson and McGarry, 2003; Johannes et al., 2017). The correlations between silt content and SPV_{tot} and between sand content and SPV_{tot} may have been consequences of the strong correlations between SOC and these properties.

Initial total specific imaged pore volume ($SPV_{Im,tot}$) was positively correlated with clay content and negatively with sand content (Fig. 5b and S1). As far as we know, these correlations have not previously been reported for soil seedbeds. However, they should perhaps be expected considering the results of previous studies on aggregate size distributions in seedbeds. For example, the extensive dataset collected by Kritz (1983) shows a strong positive correlation between clay content and the fraction of aggregates with diameters larger than 2 mm in diameter. This correlation is due to the influence of clay content on soil friability (Munkholm, 2011). For soils with low clay contents the smaller sized aggregates (<2 mm) fill up the space between the larger aggregates to a large extent, which leads to smaller inter-aggregate specific pore volumes.

The initial specific micropore volume ($SPV_{<80}$) was negatively correlated with clay content (Fig. 5a and S1), which means that higher clay content resulted in denser air-dry aggregates. The lack of (significant) correlation between clay and SPV_{tot} (Fig. S1) can be explained by the opposing effects of clay on initial $SPV_{Im,tot}$ and $SPV_{<80}$.

3.2.2. Pore network connectivity

Initial imaged pore networks were well connected compared to pore networks for more consolidated seedbeds or undisturbed soil (Jarvis et al., 2017; Sandin et al., 2017). The average initial values for the connection probability (Γ), the percolating fraction (PF) and the critical pore diameter (D_{crit}) were 0.98, 0.69 and 0.45 mm. In line with previous studies on seedbed pore networks, initial connectivity measures were positively correlated with total imaged specific pore volume ($SPV_{Im,tot}$) (Sandin et al., 2018).

3.3. Correlations between basic soil properties and changes in pore networks

Here we present results for changes in soil structural properties during the whole experiment (i.e. Drain 2-Initial). As previously shown, most of the changes occurred from the initial state to the first drainage (Fig. 4b). A complete correlation matrix for texture, SOC content,
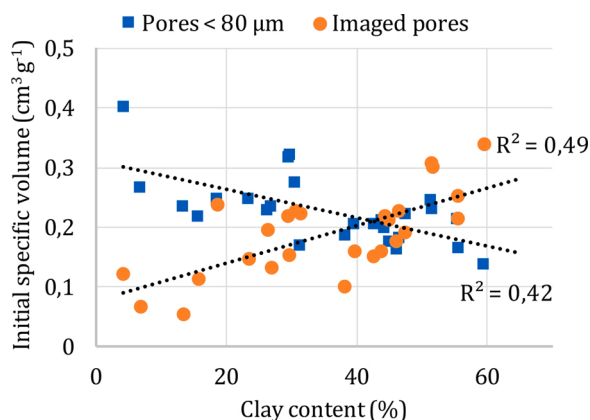
absolute changes in pore network characteristics and infiltration rate is given in Fig. 6.

3.3.1. Specific pore volumes

Both clay and SOC content generally had large effects on changes in both SPV_{tot} and pore size distributions (Fig. 6). The strongest correlation between basic soil properties and pore network characteristics found in the entire data set was between clay content and the absolute change in $SPV_{<80}$. $SPV_{<80}$ increased for all 26 samples (Figs. 6 and 7a). Larger clay contents were clearly associated with larger increases in $SPV_{<80}$. The increases in $SPV_{<80}$ ranged from 7 to 141 %. The capacity of clay soils to swell and shrink is well documented. For example, Ross (1978) showed that the coefficient of linear extensibility for a rod of soil paste ($COLE_{rod}$) between the liquid limit and air-dry state was strongly positively correlated with clay content within groups of soils with similar clay mineralogy. In turn, $COLE_{rod}$ was strongly correlated with the swelling of repacked soil immersed in water. Similar results were presented by Gray and Allbrook (2002) who studied the volume change of an aggregate between -300 cm pressure potential and oven-dry state, referred to as $COLE_{std}$, to characterize shrinkage. They showed a strong correlation between clay content and $COLE_{std}$ when they excluded soils where the clay fraction was dominated by allophanic minerals. Positive correlations between clay content and shrinking/swelling capacity have also been demonstrated for soil clods and intact soil columns (de Jong et al., 1992; Boivin et al., 2009). We did not analyze the clay mineralogy of our samples. However, clay mineralogy is rather uniform on a regional scale in Sweden (Wiklander, 1950; Eriksson et al., 2016). Most of the soils have a high content of expandable minerals (> 50 %) and mica/illite is the dominating (>20 %) non-expandable clay mineral (Eriksson, 2016). This may explain the strong correlations found in our data set. Our data, which are in line with the studies on rod, aggregate and column scales show that clay content largely governs swelling (and shrinking) also in seedbeds, at least for soils with similar clay mineralogy.

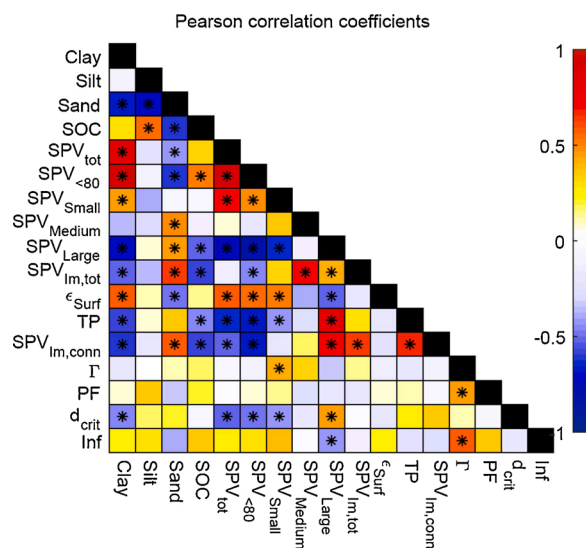The effect of SOC on soil swelling and shrinking has not been studied

Fig. 6. Pearson correlation coefficients for soil texture, SOC and absolute changes in pore network characteristics and infiltration. Asterisks indicate significant correlations (p value < 0.05). SOC, soil organic carbon content; SPV, specific pore volume; ϵ_{surf}, porosity in top 1 mm; TP, average imaged pore thickness; Γ, connection probability; PF, percolating fraction; d_{crit}, critical pore diameter; and Inf, infiltration rate at -5 cm pressure potential. The SPV subscripts refer to: <80, pores smaller than 80 µm; Small, pores between 80 and 320 µm; Medium, pores between 320 and 640 µm, Large, pores>640 µm; Im_tot, all imaged pores; Im_conn, percolating imaged pores. Rank-transformed data were used for Γ, PF, d_{crit} and Inf.

Fig. 5. Correlations between clay content and initial specific volume of pores < 80 µm and imaged pores.
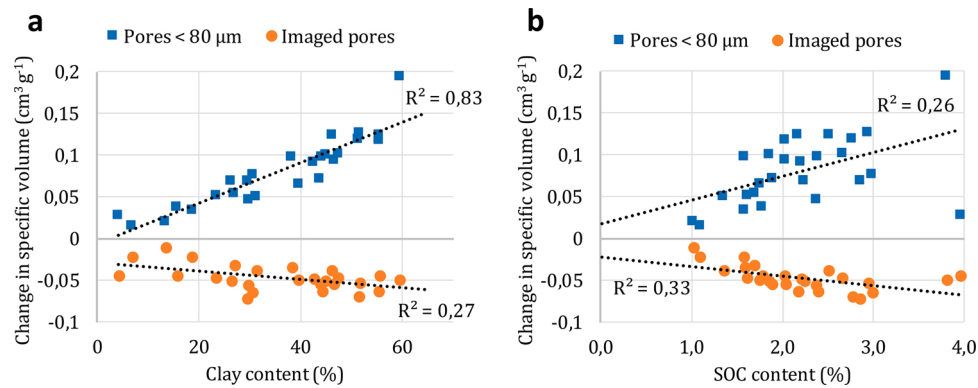
Fig. 7. Correlation between a) clay content and absolute changes in specific volume of pores < 80 μm and imaged pores and b) soil organic carbon (SOC) content and absolute changes in specific volume of pores < 80 μm and imaged pores.

as extensively as the effects of clay. Our results show a positive correlation between SOC content and the change in $SPV_{<80}$ (Figs. 6 and 7b). These results are in line with the results presented by Boivin et al. (2009) for intact soil columns.

Both clay content and SOC content have been shown to influence aggregate stability. For example Le Bissonnais et al. (1995) showed that SOC protected aggregates from breakdown both for fast (slaking) and slow wetting (micro cracking). In their study, higher clay content also led to less aggregate breakdown for slow wetting and mechanical breakdown through stirring. Similar results were also presented by Perfect et al. (1990), Le Bissonnais and Arrouays (1997) and Gronsten and Borresen (2009). More stable aggregates (i.e. soils with high clay and SOC content) should resist consolidation to a large degree. However, our data show the opposite with negative correlations both between clay content and absolute changes in $SPV_{Im,tot}$ and between SOC content and absolute changes in $SPV_{Im,tot}$ (Figs. 6 and 7). These correlations were mainly driven by the largest imaged pores (SPV_{large}). The effect of clay and SOC on the changes in $SPV_{Im,tot}$ indicates that the rearrangement of soil aggregates due to swelling was more important for consolidation than slaking and coalescence under the unsaturated experimental conditions at hand. As noted earlier initial $SPV_{Im,tot}$ was negatively correlated with clay content (Fig. 5). This means that soils with initially large $SPV_{Im,tot}$ also showed the largest decrease in $SPV_{Im,tot}$.

The changes in total specific pore volume (SPV_{tot}) were positively correlated with clay content (Figs. 6 and 7) because the increase in $SPV_{<80}$ was generally larger than the decrease in $SPV_{Im,tot}$. A similar "antagonistic" effect of SOC on pore networks of intact soil cores has previously been discussed by Boivin et al. (2009) who noted that, "The swelling of the plasma [i.e. intra-aggregate pores] will occur at the expense of the structural pore volume when the hydro-structural stability is large". Methods that can detect shifts in pore size distributions as opposed to approaches where only total porosity or bulk density are needed to enable improved process understanding.

3.3.2. Pore network connectivity

Final state (Drain 2) pore networks were generally less well connected compared to those for the initial state. The average final values for the connection probability (Γ), the percolating fraction (PF) and the critical pore diameter (d_{crit}) were 0.95, 0.60 and 0.32 mm. Again, the connectivity measures were positively correlated with total imaged specific volume for the final state (Fig. S2) which is in line with previous studies on seedbed pore networks (Sandin et al., 2018).

The changes in Γ and PF were not significantly correlated with basic soil properties while d_{crit} was weakly but significantly correlated with clay content. These results indicate that connectivity measures estimated from basic soil properties will be more uncertain than estimated measures of pore volumes. The changes in Γ and d_{crit} were correlated

with SPVs in different size classes. However, these correlations were rather weak and we, therefore, refrain from discussing these results further.

3.4. Surface porosities

Surface porosities could not be accurately determined for the Måtteby sample (Table S1) due to poor image quality at the soil surface, which for this sample was located above the cylinder walls due to swelling for all experimental stages except the initial state. Surface porosities in the uppermost 1 mm (ε_{Surf}) decreased for 23 of the remaining 25 soils for which surface porosities could be estimated, by up to 85 %. These changes are of the same magnitude as those presented by Armenise et al. (2018) and Sandin et al. (2018). Changes in ε_{Surf} were positively correlated with clay content (i.e. the decrease in ε_{Surf} was generally smaller for large clay contents) (Figs. 6 and 8a). These results indicate that, contrary to the results for changes in the whole sample (Fig. 7), swelling was not the dominating process for the changes occurring at the soil surface. All soils with a clay content above 40 % showed limited changes (Fig. 8a), which is in line with the increased aggregate strength for soils with higher clay content shown by Le Bissonnais et al. (1995). The largest decreases in ε_{Surf} were observed for two of the sandy soils and for four of the soils with silt content > 60 % (Fig. 8b). For two of these silty soils ponding of water on the soil surface occurred during the second simulated rainfall. However, the changes in ε_{Surf} were not significantly correlated with the silt content when all data points were included. Coarse textured soils have been shown to react differently to rainfall impact compared to soils of finer texture. For example coarse textured soils tend to develop structural sieving crusts while fine textured soils develop structural slaking crusts (Valentin and Bresson, 1992). It has also been shown that sandy soils may develop deeper crusts compared to finer textured soils (Armenise et al., 2018). When the three sandy soils were excluded from the dataset ε_{Surf} was negatively correlated with silt content (Fig. 8b). These results are in line with Sandin et al. (2018) who used a similar experimental setup albeit with fewer soils, and also supported by results presented by Gronsten and Borresen (2009) who showed that silty soils have less stable aggregates under wet sieving conditions. The observed negative correlation between ε_{Surf} and sand was dominated by the three sandy soils (Figs. 6 and 8c).

Changes in ε_{Surf} were not correlated with SOC (Figs. 6 and 8d) for our data set. Previous studies have shown increased aggregate stability and less surface sealing with increasing SOC content (Le Bissonnais and Arrouays, 1997; Gronsten and Borresen, 2009). The study by Gronsten and Borresen (2009) also indicated that silty soils with high SOC content (SOC > 2.3 %) had a better resistance to aggregate breakdown during wet sieving. We did not generally observe a protective effect of SOC for the silty soils included in our study. Despite SOC contents larger than 1.5
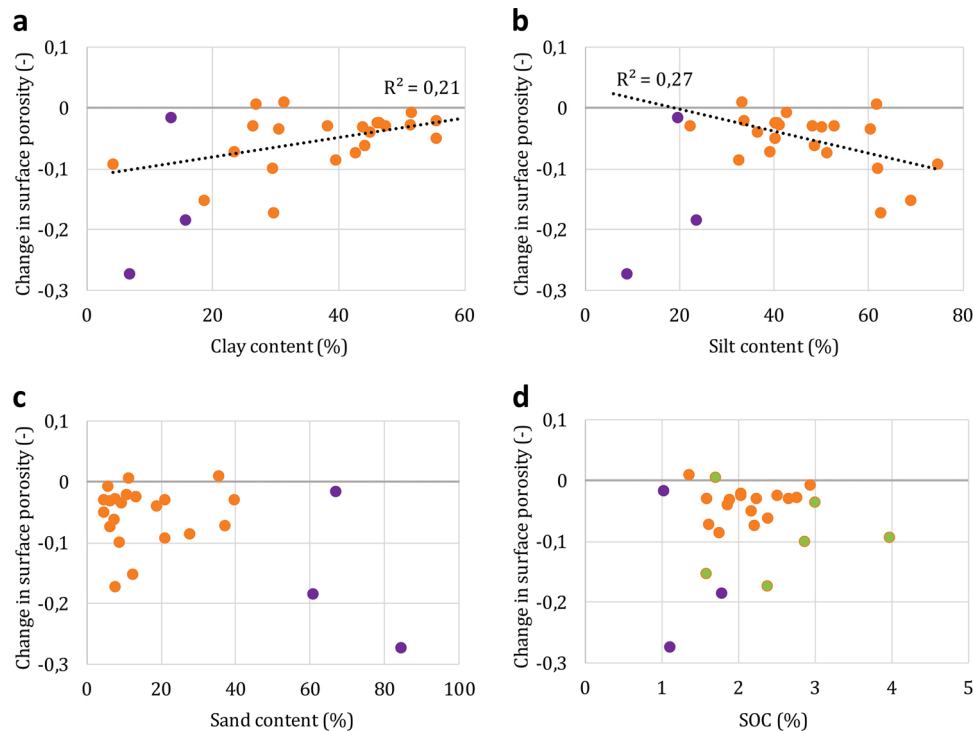
Fig. 8. Correlations between different soil properties and absolute changes in surface porosity a) clay content, b) silt content, c) sand content and d) soil organic carbon (SOC) content. The purple dots are the three sandy soils (see Figure 1) and the green dots in c are the samples with silt content > 60 %. The regression lines and accompanying R^2-values are for the data set excluding the three sandy soils.

% for all six silt dominated soils (silt content > 60 %) the decreases in ε_{Surf} were relatively large for four of these soils (Fig. 8d). Since our data set did not contain any soils with both silt content larger than 60 % and SOC content smaller than 1.5 % detection of possible effects of SOC on surface sealing of silty soils may have been hampered by the limited range of SOC contents. Future studies could examine the protective effect of SOC for Swedish soils using soils of similar texture with a large variation in SOC.

The analyzed depth (0−1 mm or 1−2 mm) did not influence the results significantly for our soils (not shown).

3.5. Infiltration rates

Measured infiltration rates do not correspond perfectly to the imaged pore networks since the pore networks may have changed during the infiltration measurement. This effect was likely larger for the initial state than the final state since final infiltration measurements were done on already consolidated soil after two cycles of rainfall and drainage. Final infiltration rates were lower than initial for 23 of the 26 soils. Initial infiltration rates were much larger for the three soils with sand content >60 % (average 64 mm h^{-1}) than for the more fine textured soils (average 6.9 mm h^{-1}). Initial infiltration rates were significantly correlated with clay and sand content and with many of the pore network characteristics. However, these correlations should be interpreted with care since they were dominated by the data for the three sandy soils and changes in pore networks may have occurred during infiltration measurements. The three sandy soils had the smallest values for initial SPV$_{Medium}$, SPV$_{Large}$, SPV$_{Im,tot}$, TP and the connectivity measures. When excluding these three soils only the positive correlation between changes in Γ, and changes in infiltration (Figs. 6 and 9), which actually became stronger, remained significant. This means that a large decrease in infiltration rate was related to a large decrease in Γ. The importance of pore network connectivity for estimating soil hydraulic conductivity has been highlighted in previous studies (e.g. Hunt, 2013; Koestel et al., 2018). However, the connection probability has generally
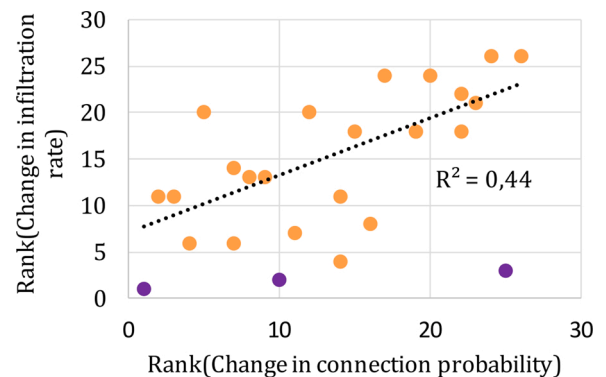

Fig. 9. Correlation between the rank of change in infiltration rate and the rank of the change in connection probability. The purple dots are the three sandy soils (see Figure 1). The regression line and accompanying R^2-value are for the data set excluding the three sandy soils.

not been included in these studies. Our results suggest that the role of the connection probability in estimating hydraulic conductivity may be worth further investigation.

4. Conclusions

With the setup used in this study (i.e. initial air-dry soil and rather slow wetting under unsaturated conditions) seedbed bulk volumes generally increased due to swelling of the intra-aggregate pore space. This swelling occurred partly at the expense of the inter-aggregate pore volume and resulted in less connected imaged pore networks. These results highlight that in order to improve the understanding of processes governing seedbed consolidation studies focusing on bulk soil are not sufficient since they would not capture the antagonistic effects of swelling on different parts of the pore space. Clay content was the most

important soil property for determining seedbed consolidation both for the intra-aggregate and inter-aggregate pore space. The major reason for this is that clay content largely determines the swelling characteristics of the soil fragments. The larger aggregate strength often associated with larger clay contents was in this study of minor importance. Modelling approaches for seedbed consolidation have up to date either been empirical or focusing on single physical processes. Although the relative importance of the processes that are active in consolidation (slaking, micro-cracking, coalescence, surface sealing) depends on the boundary condition, our results indicate that shrinking-swelling should be a central part in any model for seedbed consolidation. The results from this study provides new guidance on how basic soil properties influence seedbed consolidation, information that may be valuable for estimating model parameter values independent of modelling approach (i.e. physically based or empirical).

Declaration of Competing Interest

The authors report no declarations of interest.

Appendix A. Supplementary data

Supplementary material related to this article can be found, in the online version, at doi:https://doi.org/10.1016/j.still.2020.104849.

References

Abramoff ;, D., Magalhaes, P.J., Ram, S.J., 2004. Image processing with image. J. Biophotonics Int. 11, 36–42.

Ahuja, L.R., Ma, L.W., Timlin, D.J., 2006. Trans-disciplinary soil physics research critical to synthesis and modeling of agricultural systems. Soil Sci. Soc. Am. J. 70, 311–326.

Alletto, L., Coquet, Y., 2009. Temporal and spatial variability of soil bulk density and near-saturated hydraulic conductivity under two contrasted tillage management systems. Geoderma 152, 85–94.

Alletto, L., Pot, V., Giuliano, S., Costes, M., Perdrieux, F., Justes, E., 2015. Temporal variation in soil physical properties improves the water dynamics modeling in a conventionally-tilled soil. Geoderma 243, 18–28.

Armenise, E., Simmons, R.W., Ahn, S., Ritz, K., Garbout, A., Doerr, S.H., Mooney, S.J., Sturrock, C., Ritz, K., 2018. Soil seal development under simulated rainfall: structural, physical and hydrological dynamics. J. Hydrol. 556, 211–219. https://doi.org/10.1016/j.jhydrol.2017.10.073.

Assouline, S., 2004. Rainfall-induced soil surface sealing: A critical review of observations, conceptual models, and solutions. Vadose Zone J. 3, 570–591.

Assouline, S., Mualem, Y., 2006. Runoff from heterogeneous small bare catchments during soil surface sealing. Water Resources Res. 42, W12405.

Betzalel, I., Morin, J., Benyamini, Y., Agassi, M., Shainberg, I., 1995. Water drop energy and soil seal properties. Soil Sci. 159, 13–22.

Boivin, P., Schaeffer, B., Sturny, W., 2009. Quantifying the relationship between soil organic carbon and soil physical properties using shrinkage modelling. Eur. J. Soil Sci. 60, 265–275.

Bresson, L.M., Moran, C.J., 2004. Micromorphological study of slumping in a hardsetting seedbed under various wetting conditions. Geoderma 118, 277–288.

Chen, L., Sela, S., Svoray, T., Assouline, S., 2013. The role of soil-surface sealing, microtopography, and vegetation patches in rainfall-runoff processes in semiarid areas. Water Resources Res. 49, 5585–5599. https://doi.org/10.1002/wrcr.20360,2013.

De Jong, E., Kozak, L.M., Stonehouse, H.B., 1992. Comparison of shrink-swell indices of some Saskatchewan soils and their relationships to standard soil characteristics. Can. J. Soil Sci. 72, 429–439.

Dörner, J., Dec, D., Feest, E., Vásquez, N., Díaz, M., 2012. Dynamics of soil structure and pore functions of a volcanic ash soil under tillage. Soil Tillage Res. 125, 52–60.

Doube, M., Klosowski, M.M., Arganda-Carreras, I., Cordelieres, F.P., Dougherty, R.P., Jackson, J.S., Schmid, B., Hutchinson, J.R., Shefelbine, S.J., 2010. BoneJ free and extensible bone image analysis in image. Bone 47, 1076–1079.

Emerson, W., McGarry, D., 2003. Organic carbon and soil porosity. Aus. J. Soil Res. 41, 107–118.

Eriksson, A.K., 2016. Phosphrous speciation in agricultural clay soils. Influence of fertilization and mineralogy. PhD thesis Acta Universitatis agriculturae Sueciae 2016. Swedish University of Agricultural Sciences, Uppsala, Sweden, p. 25.

Eriksson, A.K., Hesterberg, D., Klysubun, W., Gustafsson, J.P., 2016. Phosphorus dynamics in Swedish agricultural soils as influenced by fertilization and mineralogical properties: insights gained from batch experiments and XANES spectroscopy. Sci. Total Environ. 566–567, 1410–1419.

Franzluebbers, A.J., 2002. Water infiltration and soil structure related to organic matter and its stratification with depth. Soil Tillage Res. 66 (2), 197–205.

Franzluebbers, A.J., Hons, F.M., Zuberer, D.A., 1995. Tillage-induced seasonal-changes in soil physical-properties aff ;ecting soil CO^2 evolution under intensive cropping. Soil Tillage Res. 34, 41–60.

Ghezzehei, T.A., Or, D., 2000. Dynamics of soil aggregate coalescence governed by capillary and rheological processes. Water Resources Res. 36, 367–379.

Giménez, C., Dirksen, C., Miedema, R., Eppink, L.A.A.J., Shoonderbeek, D., 1992. Surface sealing and hydraulic conductances under varying-intensity rains. Soil Sci. Soc. Am. J. 56, 234–242.

Gray, C.W., Allbrook, R., 2002. Relationships between shrinkage indices and soil properties in some New Zealand soils. Geoderma 108, 287–299.

Gronsten, H.A., Borresen, T., 2009. Comparison of two methods for assessment of aggregate stability of agricultural soils in southeast Norway. Acta Agric. Scand. Section B - Soil and Plant Sci. 59 (6), 567–575. https://doi.org/10.1080/09064710802495356.

Gupta, S.D., Mohanty, B.P., Kohne, J.M., 2006. Soil hydraulic conductivities and their spatial and temporal variations in a vertisol. Soil Sci. Soc. Am. J. 70, 1872–1881.

Hiel, M.-P., Chélin, M., Parvin, N., Barbieux, S., Degrune, F., Lemtiri, A., Colinet, G., Degré, A., Bodson, B., Garrré, S., 2016. Crop residue management in arable cropping systems under a temperate climate. Part 2: Soil physical properties and crop production. A review. Biotech. Agron. Soc. Environ. 20, 245–256.

Hunt, A.G., Ewing, R.P., Horton, R., 2013. What's wrong with soil physics? Soil Sci. Soc. Am. J. 77, 1877–1887.

Hyvaluoma, J., Thapaliya, M., Alaraudanjoki, J., Siren, T., Mattila, K., Timonen, J., Turtola, E., 2012. Using microtomography, image analysis and flow simulations to characterize soil surface seals. Comp. Geosci. 48, 93–101.

Jarvis, N., Larsbo, M., Koestel, J., 2017. Connectivity and percolation of structural pore networks in a cultivated silt loam soil quantified by X-ray tomography. Geoderma 287, 71–79.

Johannes, A., Matter, A., Schulin, R., Weisskopf, P., Baveye, P., Boivin, P., 2017. Optimal organic carbon values for soil structure quality of arable soils. Does clay content matter? Geoderma 302, 14–21.

Kätterer, T., Andrén, O., Jansson, P.E., 2006. Pedotransfer functions for estimating plant available water and bulk density in Swedish agricultural soils. Acta Agric. Scand. B Soil Plant Sci. 56, 263–276.

Koestel, J., 2018. SoilJ: an ImageJ Plugin for the semiautomatic processing of three-dimensional X-ray images of soils. Vadose Zone J. https://doi.org/10.2136/vzj2017.03.006.

Koestel, J., Dathe, A., Skaggs, T.H., Klakegg, O., Ahmad, M.A., Babko, M., Gimenez, D., Farkas, C., Nemes, A., Jarvis, N., 2018. Estimating the permeability of naturally structured soil from percolation theory and pore space characteristics imaged by X-Ray. Water Resources Res. 54, 9255–9263.

Kritz, G., 1983. Physical Conditions in Cereal Seedbeds: A Sampling Investigation in Swedish Spring-sown Fields. ISSN: 0348-0976. ISBN: 91-576-1558-6.

Le Bissonnais, Y., Arrouays, D., 1997. Aggregate stability and assessment of soil crustability and erodibility. 2. Application to humic loamy soils with various organic carbon contents. Eur. J. Soil Sci. 48, 39–48.

Le Bissonnais, Y., Renaux, B., Delouche, H., 1995. Interactions between soil properties and moisture content in crust formation, runoff and interrill erosion from tilled loess soils. Catena 25, 33–46.

Lin, H., 2011. Three principles of soil change and pedogenesis in time and space. Soil Sci. Soc. Am. J. 75, 2049–2070.

Löv, Å., Sjöstedt, C., Larsbo, M., Persson, I., Gustafsson, J.P., Cornelis, G., Kleja, D.B., 2017. Solubility and transport of Cr (III) in a historically contaminated soil – evidence of a rapidly reacting dimeric Cr (III) organic matter complex. Chemosphere 189 (Supplement C), 709–716.

Maharjan, G.R., Prescher, A.-K., Nendel, C., Ewert, F., Mboh, C.M., Gaiser, T., Seidel, S.J., 2018. Approaches to model the impact of tillage implements on soil physical and nutrient properties in different agro-ecosystem models. Soil Tillage Res. 180, 210–221.

Mamedov, A.I., Levy, G.J., 2013. High energy moisture characteristics: linking between some soil physical processes and structure stability. In: Logsdon, S., Berli, M., Horn, R. (Eds.), Quantifying and Modeling Soil Structure Dynamics 3, 41–74, 3.

Messing, I., Jarvis, N.J., 1993. Temporal variation in the hydraulic conductivity of a tilled clay soil as measured by tension infiltrometers. Eur. J. Soil Sci. 44, 11–24. https://doi.org/10.1111/j.1365-2389.1993.tb00430.x.

Munkholm, L.J., 2011. Soil friability: a review of the concept, assessment and effects of soil properties and management. Geoderma 167-168, 236–246.

Or, D., Ghezzehei, T.A., 2002. Modeling post-tillage soil structural dynamics: a review. Soil Tillage Res. 64, 41–59.

Or, D., Leij, F.J., Snyder, V., Ghezzehei, T.A., 2000. Stochastic model for post tillage soil pore space evolution. Water Resources Res. 36, 1641–1652.

Otsu, N., 1979. Threshold selection method from grey-level histograms. IEEE Trans. Syst. Man Cyb. 9, 62–66.

Perfect, E., Kay, B.D., Vanloon, W.K.P., Sheard, R.W., Pojasok, T., 1990. Factors influencing soil structural stability within a growing-season. Soil Sci. Soc. Am. J. 54, 173–179.

R Core Team, 2019. R: A Language and Environment for Statistical Computing. URL. Foundation for Statistical Computing, Vienna, Austria. https://www.R-project.org/.

Ramos, M.C., Nacci, S., Pla, I., 2003. Effect of raindrop impact and its relationship with aggregate stability to different disaggregation forces. Catena 53, 365–376.

Renard, P., Allard, D., 2013. Connectivity metrics for subsurface flow and transport. Adv. in Water Resources 51, 168–196.

Ross, G.J., 1978. Relationships of specific surface area and clay content to shrink-swell potential of soils having different clay mineralogical compositions. Can. J. Soil Sci. 58, 159–166.

Ruhlmann, J., Korschens, M., Graefe, J., 2006. A new approach to calculate the particle density of soils considering properties of the soil organic matter and the mineral matrix. Geoderma 130, 272–283.

Salles, C., Poesen, J., Govers, G., 2000. Statistical and physical analysis of soil detachment by raindrop impact: rain erosivity indices and threshold energy. Water Resources Res. 36, 2721–2729.

Sandin, M., Koestel, J., Jarvis, N., Larsbo, M., 2017. Post-tillage evolution of structural pore space and saturated and near-saturated hydraulic conductivity in a clay loam soil. Soil Tillage Res. 165, 161–168.

Sandin, M., Jarvis, N., Larsbo, M., 2018. Consolidation and surface sealing of nine harrowed Swedish soils. Soil Tillage Res. 181, 82–92.

Schindelin, J., Arganda-Carreras, I., Frise, E., Kaynig, V., Longair, M., Pietzsch, T., Preibisch, S., Rueden, C., Saalfeld, S., Schmid, B., Tinevez, J.Y., White, D.J., Hartenstein, V., Eliceiri, K., Tomancak, P., Cardona, A., 2012. Fiji: an open-source platform for biological-image analysis. Nat. Methods 9, 676–682.

Schwen, A., Bodner, G., Scholl, P., Buchan, G.D., Loiskandl, W., 2011. Temporal dynamics of soil hydraulic properties and the water-conducting porosity under diff ; erent tillage. Soil Tillage Res. 113, 89–98.

Valentin, C., Bresson, L.M., 1992. Morphology, genesis and classification of surface crusts in loamy and sandy soils. Geoderma 55 (3-4), 225–245.

van Dijk, A.I.J.M., Bruijnzeel, L.A., Rosewell, C.J., 2002. Rainfall intensity-kinetic energy relationships: a critical literature appraisal. J. Hydrol. 261, 1–23.

Wiklander, L., 1950. Mineralogical composition of quaternary Swedish clays. Nature 166, 276–277.